

# Southern Ocean warming delayed by circumpolar upwelling and equatorward transport

Kyle C. Armour<sup>1\*</sup>, John Marshall<sup>2</sup>, Jeffery R. Scott<sup>2,3</sup>, Aaron Donohoe<sup>4</sup> and Emily R. Newsom<sup>5</sup>

**The Southern Ocean has shown little warming over recent decades, in stark contrast to the rapid warming observed in the Arctic. Along the northern flank of the Antarctic Circumpolar Current, however, the upper ocean has warmed substantially. Here we present analyses of oceanographic observations and general circulation model simulations showing that these patterns—of delayed warming south of the Antarctic Circumpolar Current and enhanced warming to the north—are fundamentally shaped by the Southern Ocean's meridional overturning circulation: wind-driven upwelling of unmodified water from depth damps warming around Antarctica; greenhouse gas-induced surface heat uptake is largely balanced by anomalous northward heat transport associated with the equatorward flow of surface waters; and heat is preferentially stored where surface waters are subducted to the north. Further, these processes are primarily due to passive advection of the anomalous warming signal by climatological ocean currents; changes in ocean circulation are secondary. These findings suggest the Southern Ocean responds to greenhouse gas forcing on the centennial, or longer, timescale over which the deep ocean waters that are upwelled to the surface are warmed themselves. It is against this background of gradual warming that multidecadal Southern Ocean temperature trends must be understood.**

The surface of the Southern Ocean (SO), poleward of the Antarctic Circumpolar Current (ACC), has warmed by 0.02 °C per decade since 1950, whereas global-mean sea-surface temperature (SST) has increased by 0.08 °C per decade (Methods and Supplementary Fig. 1). Slow warming of the SO in response to greenhouse gas (GHG) forcing is also a ubiquitous feature of comprehensive general circulation model (GCM) simulations<sup>1–7</sup>. Yet, both palaeoclimate observations<sup>8</sup> and GCMs<sup>4</sup> show polar amplification in the Southern Hemisphere—with warming in the SO comparable to that in the Arctic—at millennial timescales. That is, SO warming emerges rather slowly, but may become substantial.

Delayed warming of the SO has been widely attributed to a large thermal inertia arising from storage of heat within very deep mixed layers<sup>1–4,6,8–10</sup>. However, this link rests primarily on pioneering studies of climate change<sup>1,2</sup> using early GCMs with crude representations of eddies and mixing that produced too much deep convection throughout the SO<sup>11</sup>—suggesting that the role of vertical mixing has been overemphasized. Indeed, delayed SO warming robustly occurs within recent generations of GCMs that simulate more realistic convection<sup>11</sup> and shallow SO mixed layers<sup>12</sup>. Moreover, the deepest mixed layers do not coincide with regions of delayed warming but, instead, are found<sup>12</sup> within and just north of the ACC (40°–50° S), where SSTs have been increasing rapidly (0.11 °C per decade since 1950).

Several other processes have also been suggested. Near Antarctica, where a persistent halocline exists, freshening of the upper ocean can decrease SSTs by weakening convection and vertical mixing, thus reducing the upward flux of heat from relatively warm waters at depth<sup>1,13–15</sup>. A strengthening and poleward shift of the surface westerlies—driven by stratospheric ozone depletion<sup>16</sup>—

may also act to cool the region south of the ACC through enhanced advection of cold surface waters northwards<sup>16–18</sup>. Moreover, the SO sea surface may be shielded from radiative forcing, either by extensive sea-ice cover<sup>19</sup> or by increased low-cloud reflectivity through enhanced wind-driven emissions of sea spray<sup>20</sup>. In this study, guided by observations and a hierarchy of models, we find that, although the above processes may play a role, the primary source of delayed SO warming is the background ocean circulation.

Substantial progress has been made in understanding the SO's meridional overturning circulation (MOC)<sup>21</sup>, with its upwelling branch as a balance between wind-driven (Eulerian-mean,  $\bar{\psi}$ ) and eddy-induced ( $\psi^*$ ) advection: surface-wind stresses produce strong circumpolar upwelling south of the zonal-mean wind maximum (near 52° S), equatorward surface flow, and downwelling to the north; mesoscale eddy fluxes flatten the density surfaces that have been tilted by the winds, inducing a compensating circulation<sup>21</sup>. The resulting, 'residual-mean' flow ( $\psi_{\text{res}} = \bar{\psi} + \psi^*$ ) is a broad upwelling along sloped isopycnals and equatorward transport at the surface<sup>21,22</sup>—evident in the transport of cold and fresh surface waters from the region of seasonal sea ice to subduction zones on the northern flank of the ACC (Fig. 1d). The SO's residual-mean MOC has become recognized as a key component of the global ocean circulation and climate system<sup>21</sup>. Here, we show the MOC plays a similarly fundamental role in the SO's response to climate forcing.

## Delayed Southern Ocean warming in observations

Our observational analysis covers the period 1982–2012, for which both *in situ* and satellite observations of SSTs<sup>23</sup> and sea-surface heat fluxes<sup>24</sup> (SHFs) are available, and ocean temperature measurements<sup>25,26</sup> have reasonable coverage within the SO

<sup>1</sup>School of Oceanography and Department of Atmospheric Sciences, University of Washington, Seattle, Washington 98195, USA. <sup>2</sup>Department of Earth, Atmospheric and Planetary Sciences, Massachusetts Institute of Technology, Cambridge, Massachusetts 02139, USA. <sup>3</sup>Center for Global Change Science, Massachusetts Institute of Technology, Cambridge, Massachusetts 02139, USA. <sup>4</sup>Polar Science Center, Applied Physics Laboratory, University of Washington, Seattle, Washington 98195, USA. <sup>5</sup>Department of Earth and Space Sciences, University of Washington, Seattle, Washington 98195, USA.

\*e-mail: karmour@uw.edu

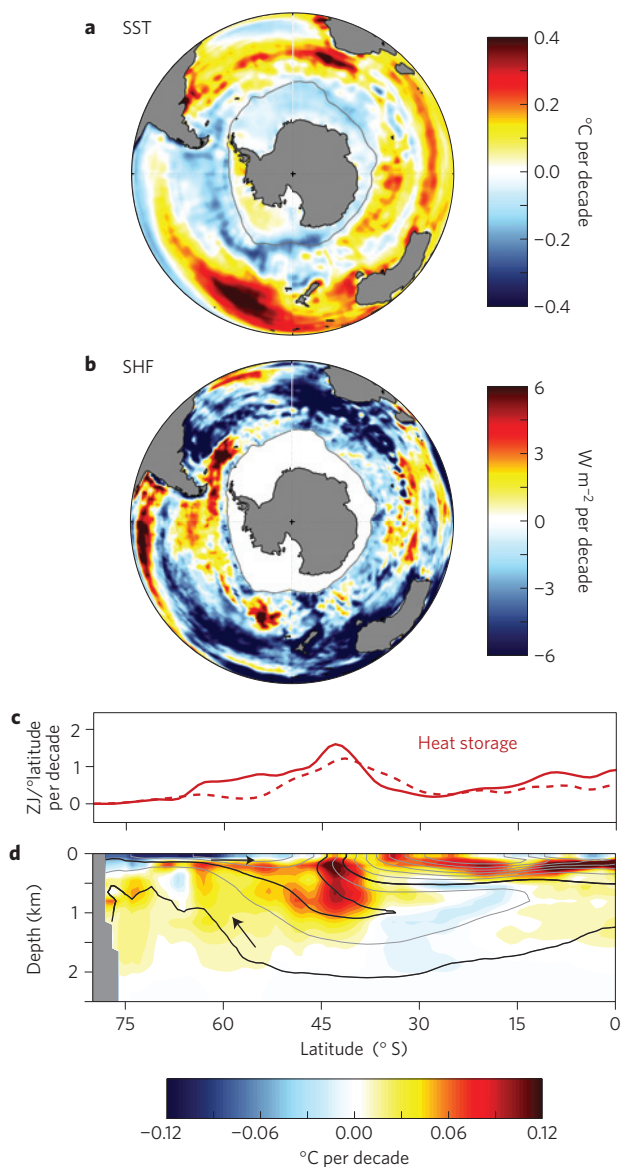


**Figure 1 | Observed trends over 1982–2012.** **a**, Annual-mean SST trend. **b**, Net SHF trend (positive into ocean). **c**, Zonally and depth-integrated ocean heat content trends from two different subsurface temperature data sets: EN4 (solid; ref. 25) and Ishii (dashed; ref. 26). **d**, Zonal-mean ocean potential temperature trend from EN4, with contours of climatological ocean salinity in intervals of 0.15 practical salinity units (psu) (grey lines). Arrows indicate the orientation of the residual-mean MOC following ref. 22, along 34.4 and 34.7 psu contours (black lines). Grey line in **a** and **b** shows maximum winter sea-ice extent from ref. 24.

(Methods). Rapid surface warming occurs in zonal bands along the ACC's northern flank, with slower warming and cooling to the south (Fig. 1a). These SST patterns are mirrored by trends in zonal-mean ocean temperature and depth-integrated heat content (Fig. 1c,d); the greatest warming occurs in the vicinity of the ACC (40°–50° S)—consistent with observed trends since the 1950s<sup>27,28</sup>. This structure of ocean warming is robust across subsurface temperature data sets and ocean reanalyses, and is consistent with satellite altimetry measurements that show rapid sea-level rise in the vicinity of the ACC and little sea-level rise to the south<sup>29,30</sup> (Fig. 1c and Supplementary Figs 2–4).

The SHF observations are comprised of turbulent fluxes of sensible and latent heat estimated from bulk formulae, as well as

surface radiation derived from satellite observations<sup>24</sup>. Although these SHFs are limited in accuracy<sup>24,28</sup> and spatial coverage (with no observations available under sea ice), they provide valuable insight into the causes of the observed changes. We see that regions that have warmed strongly have increasingly lost heat to the atmosphere, whereas regions that have warmed less (or cooled) have increasingly taken up heat (Fig. 1a,b). These SHF patterns primarily reflect trends in sensible and latent heat fluxes (Supplementary Fig. 5) which, in turn, have been driven by changing air–sea temperature gradients: anomalous surface heat uptake has mainly occurred south of the ACC, where the atmosphere has warmed more rapidly than the ocean surface; anomalous surface heat loss has occurred in the vicinity of the ACC and to the north, where the ocean surface has warmed more rapidly than the atmosphere (Supplementary Fig. 6). That is, SHFs seem to have damped—not driven—the spatial pattern of SST trends.

Moreover, the spatial patterns of SHF and depth-integrated ocean heat content trends are largely opposed over the SO, with the regions of greatest (least) surface heat uptake showing the least (greatest) amount of heat storage (Fig. 1b,c and Supplementary Figs 2–4). This suggests that meridional ocean heat transport (OHT) changes—rather than vertical heat redistribution or SHFs—have predominantly shaped the pattern of SO warming. Indeed, it seems that a portion of the heat taken up poleward of the ACC has been transported northwards, instead of being stored locally, and converged along the ACC's northern flank. This mirrors the climatological northward transport and subduction of surface waters, consistent with the strong correspondence between the background MOC and the pattern of ocean warming (Fig. 1d).

These observations suggest that anomalous transport of heat by the MOC has damped warming south of the ACC and enhanced warming to the north. However, subsurface temperature observations are sparse over the SO, particularly south of the ACC<sup>27,31</sup>, and uncertainties in SHF observations are substantial<sup>24,28</sup> (Supplementary Fig. 7). Therefore, to quantitatively study the mechanisms driving delayed SO warming, we turn our focus to numerical climate model simulations.

### Delayed Southern Ocean warming in climate models

We first consider the ensemble of comprehensive GCMs participating in phase 5 of the Coupled Model Intercomparison Project<sup>32</sup> (CMIP5) driven by historical radiative forcing (Methods). The CMIP5 models broadly capture the observed changes over 1982–2012, with little surface warming poleward of the ACC and bands of rapid warming along its northern flank (Fig. 2a). The GCMs simulate slightly more Southern Hemispheric ocean heat storage ( $0.64 \pm 0.21 \text{ W m}^{-2}$ ) than is observed over this period ( $0.4\text{--}0.6 \text{ W m}^{-2}$ ; Supplementary Information), possibly owing to model deficiencies or to observational biases introduced by infilling data-sparse regions of the ocean<sup>27,31</sup>. Yet, they robustly capture the patterns of heat storage, with substantial warming in the vicinity of the ACC and less warming to the south (Fig. 2c,e). Moreover, the spatial pattern of SHF trends broadly opposes the pattern of SST trends (Fig. 2a,b), with local turbulent heat flux trends reaching several  $\text{W m}^{-2}$  per decade—an order of magnitude larger than radiative forcing trends over this period.

The region of delayed SO warming, poleward of 50° S, accounts for  $60 \pm 10\%$  of hemispheric surface heat uptake, but only  $23 \pm 6\%$  of hemispheric heat storage (Fig. 2c). That is, less than one third of the anomalous heat taken up at the surface is stored locally; the majority ( $68 \pm 11\%$ ) is transported northwards, as seen by the robust increase in northward OHT across the ACC (Fig. 2d and Methods). Meanwhile, less than half of the heat stored on the equatorward flank of the ACC (40°–50° S) is derived from local surface heat uptake; the rest is due to convergence of heat by the ocean. These patterns are broadly consistent with previous modelling

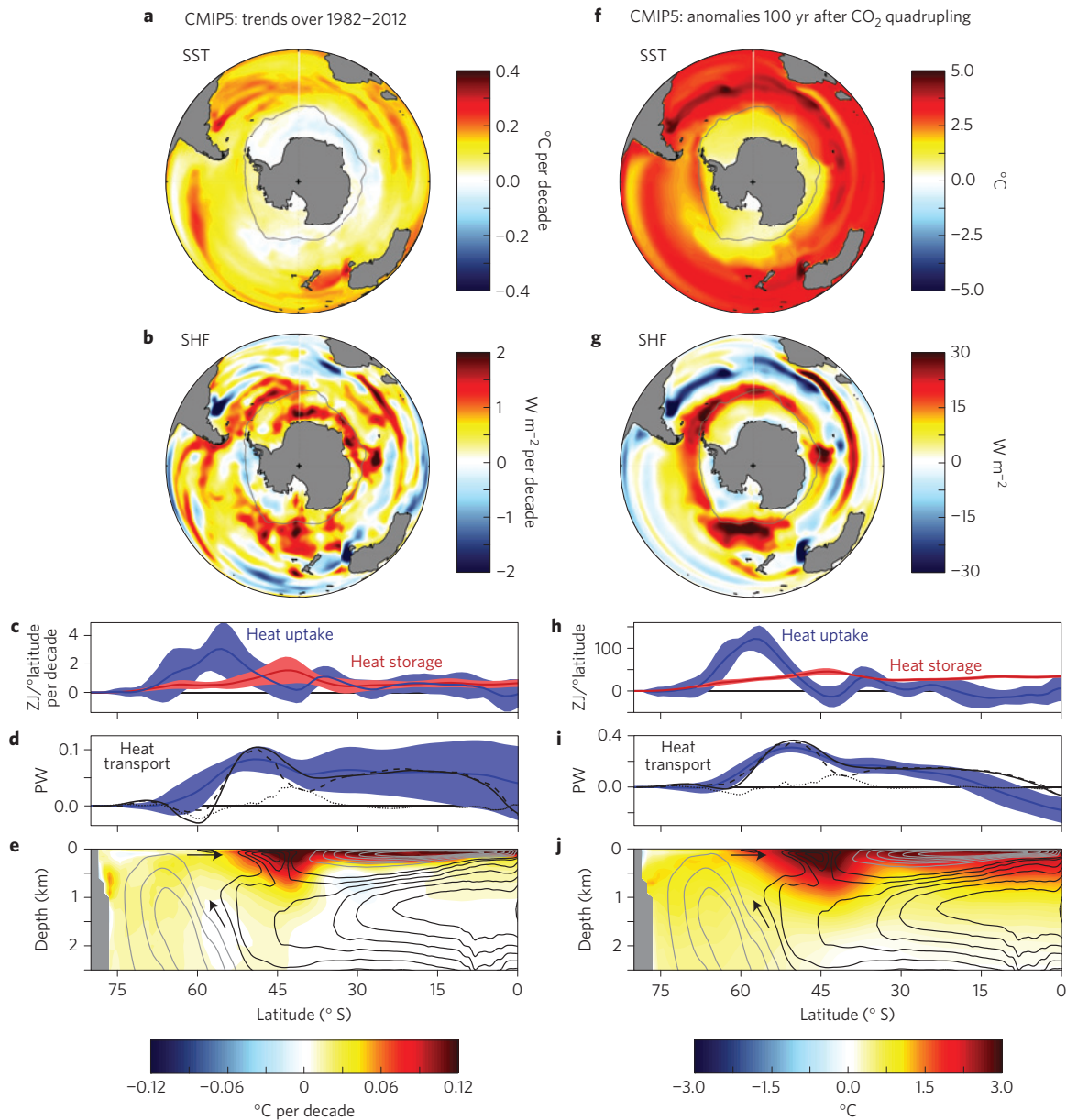


**Figure 2 |** CMIP5-mean trends over 1982–2012 (left) and response to CO<sub>2</sub> forcing (right). **a**, Annual-mean SST trend. **b**, Net SHF trend (positive into ocean). **c**, Zonally integrated average SHF (blue) and full-depth ocean heat content trend (red). **d**, Anomalous OHT for CMIP5-mean (blue) and CCSM4 (black; solid, dashed and dotted lines show total, residual-mean advection and diffusion, respectively). **e**, Zonal-mean ocean potential temperature trend, with contours showing the MOC from CCSM4 (black contours show positive circulation in 4 Sv increments, grey contours show negative circulation in –4 Sv increments). **f–j**, As in **a–e**, but anomalies over 100 yr in response to abrupt CO<sub>2</sub> quadrupling. Grey line in **a, b, f** and **g** shows maximum winter sea-ice extent, as in Fig. 1. Shading in **c, d, h** and **i** shows the ±1 s.d. range across the CMIP5 models; these ranges are broader than those from internal variability alone (Supplementary Fig. 9).

studies<sup>33–35</sup> and the observations (Fig. 1). From an energetics perspective, then, delayed SO warming is primarily driven by increased northward OHT across the ACC, and enhanced warming in the vicinity of the ACC is driven, in large part, by oceanic heat flux convergence.

A key question is, what dynamics give rise to these OHT changes? Within and to the south of the ACC, wind-driven gyres contribute little to meridional OHT, and thus we can make the approximation<sup>36</sup>:  $OHT \approx \rho c_p \psi_{res} \Delta T + R$ , where  $\psi_{res} = \bar{\psi} + \psi^*$  is the strength of the residual-mean MOC;  $\Delta T$  is the vertical temperature difference between northward and southward flowing branches of the MOC;  $\rho$  and  $c_p$  are the density and specific heat of sea water, respectively; and  $R$  represents diffusion of heat

along isopycnal surfaces. For visual guidance, we calculate  $\psi_{res}$  from the National Center for Atmospheric Research’s CCSM4 (Methods). As in the observations, there is a striking similarity between this background residual-mean MOC and the pattern of ocean warming (Fig. 2e). Moreover, OHT changes arise almost entirely from anomalous advection of heat by the residual-mean circulation; changes in the isopycnal diffusion of heat are relatively small (Fig. 2d).

To further reveal the dynamics underlying these advective OHT changes, we consider a series of idealized GCM simulations aimed at removing the influence of particular climate processes. We first examine the long-term response of the CMIP5 GCMs to GHG forcing alone—at a century following an abrupt quadrupling of CO<sub>2</sub>



(Fig. 2f–j). Although westerly wind changes in these simulations may initially act to cool the SO by advecting cold surface waters northwards<sup>16–18</sup>, they ultimately drive enhanced warming south of the ACC (after several years to several decades) as poleward eddy heat fluxes increase<sup>18,37</sup> and relatively warm waters at depth are upwelled at a greater rate<sup>7,37–40</sup>. That is, wind changes do not contribute to delayed SO warming at the centennial timescale considered here. Yet, the patterns and mechanisms of SO changes under GHG forcing are remarkably similar to those over the historical period: warming is damped poleward of the ACC and enhanced within zonal bands along its northern flank (Fig. 2f); and although the region poleward of 50° S accounts for nearly all (95 ± 21%) of the hemispheric heat uptake over the century (Fig. 2h), the majority (67 ± 5%) of this heat is advected northwards by residual-mean currents and converged equatorward of the ACC (Fig. 2i). This suggests that although atmospheric circulation changes may partially account<sup>7</sup> for differences between the historical simulations (Fig. 2a–e) and observations (Fig. 1), they do not play a critical role in delayed SO warming. Instead, delayed SO warming—driven by anomalous northward OHT—seems to be a fundamental ocean response to GHG forcing.

### Delayed Southern Ocean warming in an ocean-only model

We can further clarify the dynamics of delayed SO warming by simulating GHG forcing within an ocean-only GCM. In particular, we simulate the global ocean with the MITgcm<sup>41,42</sup>, and produce a climate change scenario by applying a constant radiative forcing of  $F = 4 \text{ W m}^{-2}$  uniformly over the sea surface (including under sea ice)—approximating the radiative effect of an abrupt doubling of CO<sub>2</sub> (Methods). This GHG forcing is prescribed concurrently with constant, annually repeating sea-surface buoyancy and momentum fluxes that have been derived from a long ‘control’ simulation (see Methods and ref. 43 for details). We further specify a spatially uniform ‘radiative feedback’ on SST anomalies (relative to the control) with value  $\lambda = 1 \text{ W m}^{-2} \text{ } ^\circ\text{C}^{-1}$ , representing the additional energy emitted to space as the surface warms; this value is characteristic of feedbacks found within the CMIP5 GCMs and estimated from satellite observations<sup>44</sup>. Equilibrium would thus be reached when the global-mean SST increases by  $F/\lambda = 4 \text{ } ^\circ\text{C}$ , such that the global radiative response balances the radiative forcing. However, the magnitude of warming need not be the same everywhere. Importantly, because  $F$  and  $\lambda$  are geographically uniform, and all other sea-surface fluxes are held fixed at their control values, any spatial structure in the response can be wholly attributed to oceanic processes.

This ocean-only framework thus mimics GHG-induced warming under the idealizations that: there is no change in atmospheric heat transport; radiative forcing and feedbacks are spatially uniform; and there are no changes in surface winds or freshwater fluxes. Remarkably, the ocean-only GCM captures the principal features of Figs 1 and 2, including delayed warming poleward of the ACC and enhanced warming within zonal bands along its northern flank (Fig. 3a,e). Moreover, the mechanism shaping the SO response is the same: the majority (73%) of the heat taken up poleward of 50° S is advected northwards by residual-mean currents and converged equatorward of the ACC (Fig. 3c,d). Delayed SO warming is thus a general feature of the ocean’s response to GHG forcing—independent of geographic variations in radiative forcing or feedbacks, trends in atmospheric circulation, or changes in freshwater fluxes.

What role do ocean circulation changes play in delayed SO warming? To address this question, we consider the response of the ocean-only GCM to a passive, dye-like tracer applied at the sea surface (similar in spirit to refs 14,45). The simulation is designed to be analogous to the GHG-forcing scenario above, except that ocean circulation is unchanged and the tracer is advected and mixed

from the surface only by climatological ocean processes (Methods). Directly comparing the passive-tracer response (Fig. 3f–j) and the GHG-induced response (Fig. 3a–e) reveals the role of ocean circulation changes.

The passive-tracer simulation captures the broad features of the SO’s response to GHG forcing, with delayed SO warming arising from the advection of the anomalous warming signal by climatological ocean currents. That is, OHT changes can be largely understood as a change in the vertical temperature profile (Fig. 3e,j) on which the climatological residual-mean MOC acts ( $\psi_{\text{res}} \Delta T'$ ): greater warming near the surface (where the flow is northward) than at depth (where the flow is southward) results in anomalous northward OHT that nearly balances anomalous surface heat uptake south of the ACC; in turn, warming is damped south of the ACC and enhanced to the north (Fig. 3d,i). Equivalently, delayed SO warming can be viewed as arising from the equatorward transport of surface waters that have not yet been exposed to GHG forcing, with deep waters that have not yet been modified by GHG forcing being upwelled in their place (Fig. 3e,j).

Two notable differences between the GHG and passive-tracer simulations are the depth over which anomalous heat is stored in the ocean (Fig. 3e,j and Supplementary Fig. 10) and the structure of warming near the ACC (Fig. 3a,f). Both can be linked to enhanced stratification of the upper ocean under GHG-induced heat uptake (absent under passive-tracer uptake). The zonal bands of warming within subduction regions north of the ACC are driven by a shoaling of winter mixed layers under warming (Supplementary Fig. 11), leading to a reduction in mode water formation<sup>46</sup> and enhanced heat storage near the surface. These findings suggest that rapid warming and sea-level rise along the northern flank of the ACC do not require a wind-driven shift of ocean fronts, as has been assumed<sup>17,18,27,33</sup> but not observed<sup>47</sup>, and may instead be due to a convergence of heat that was taken up south of the ACC.

Additional ocean-only simulations show that surface westerly changes drive SO cooling on sub-decadal timescales, but ultimately enhance SO warming after several decades (Supplementary Figs 12 and 14). Moreover, freshwater forcing simulations suggest that changes in the hydrologic cycle produce only modest cooling south of the ACC (Supplementary Figs 13 and 14). These results are consistent with the results of wind<sup>17,37–40</sup> and freshwater<sup>48,49</sup> forcing simulations with coupled GCMs.

Observations and a hierarchy of GCM simulations show that delayed warming of the SO, poleward of the ACC, is a fundamental consequence of circumpolar upwelling and equatorward transport of surface waters by the SO’s climatological residual-mean MOC. Spatial variations in mixed layer depths, patterns of radiative forcing and feedbacks, changes in the hydrologic cycle, and changes in atmospheric and oceanic circulations all seem to play a secondary role in shaping the SO response to GHG-induced warming. These results suggest that although ocean heat uptake curbs surface warming at the global scale, the slow pace of warming in the SO is instead due to meridional OHT changes driven by regional ocean circulations; in turn, heat uptake peaks in the SO because the sea surface warms slowly relative to the overlying atmosphere.

These findings further suggest that warming of the SO surface is set by the time it takes for deep ocean waters—originating in the North Atlantic Ocean and ultimately upwelled to the SO surface<sup>21</sup>—to be warmed themselves. This implies a timescale of multiple centuries for the SO to respond to GHG forcing, consistent with the slow pace of SO warming seen in observations and GCM simulations<sup>3,4,8</sup>. Although these results do not explain the observed cooling of the SO over the most recent few decades (Fig. 1a), they suggest that this trend, and its driving mechanisms, must be understood against a background of gradual GHG-induced warming—instead of the rapid warming observed in the Arctic.

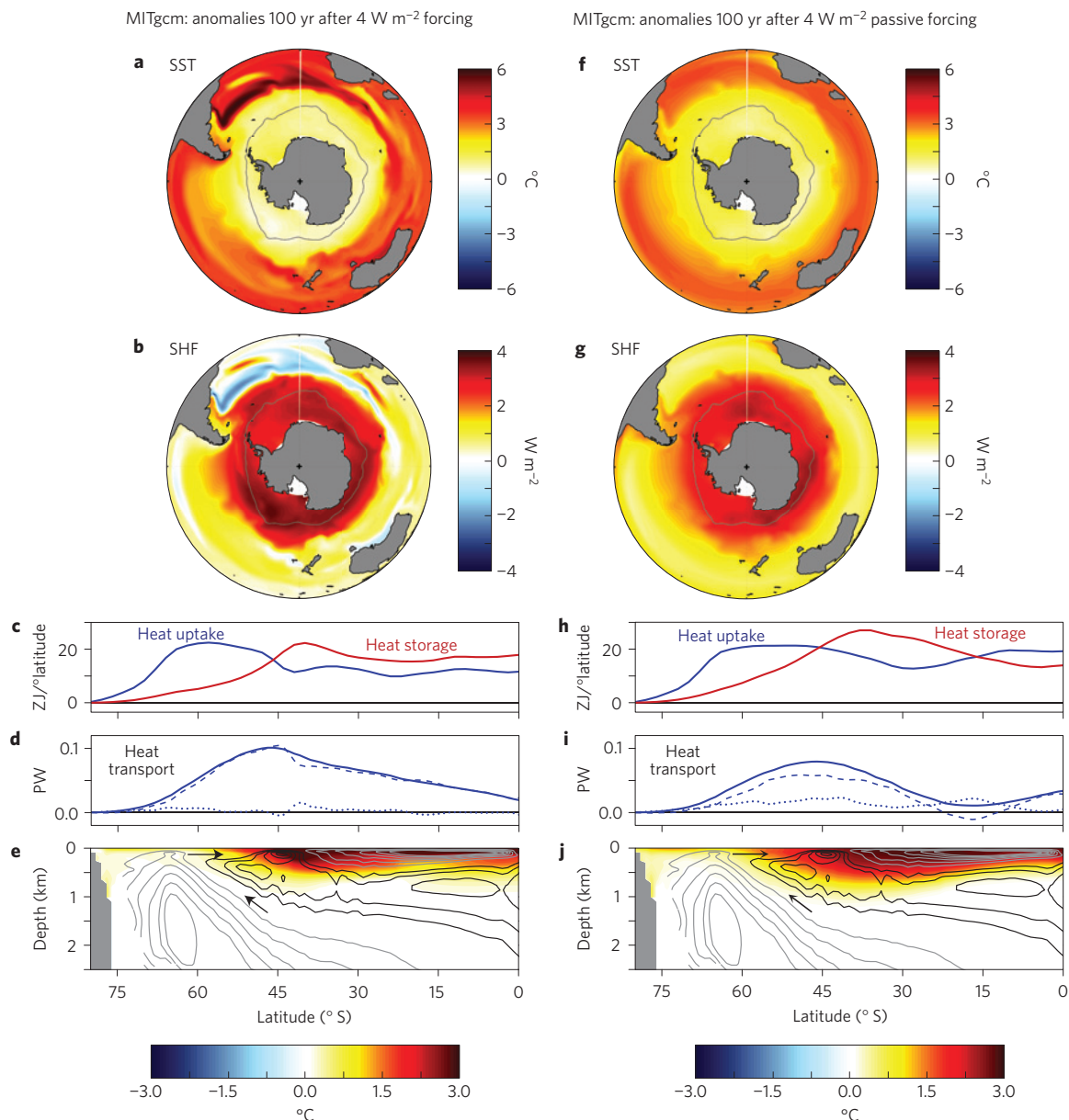


**Figure 3 | MITgcm response to uniform GHG forcing (left) and passive-tracer forcing (right).** **a**, Annual-mean SST anomaly. **b**, Net SHF anomaly (positive into ocean). **c**, Zonally integrated average SHF anomaly (blue) and full-depth ocean heat content anomaly (red). **d**, Anomalous OHT (solid, dashed and dotted lines show total, residual-mean advection and diffusion, respectively). **e**, Zonal-mean ocean potential temperature anomaly, with contours showing the MOC from the control simulation (black contours show positive circulation in 2 Sv increments, grey contours show negative circulation in -4 Sv increments). **f-j**, As in **a-e**, but for the passive-tracer simulation. Grey line in **a,b,f** and **g** shows maximum winter sea-ice extent, as in Fig. 1.

**Methods**

Methods, including statements of data availability and any associated accession codes and references, are available in the online version of this paper.

Received 20 February 2016; accepted 4 May 2016; published online 30 May 2016

**References**

1. Manabe, S., Bryan, K. & Spelman, M. J. Transient response of a global ocean-atmosphere model to a doubling of atmospheric carbon dioxide. *J. Phys. Oceanogr.* **20**, 722–749 (1990).
2. Manabe, S., Stouffer, R. J., Spelman, M. J. & Bryan, K. Transient responses of a coupled ocean-atmosphere model to gradual changes of atmospheric CO<sub>2</sub>. Part 1: Annual mean response. *J. Clim.* **4**, 785–818 (1991).
3. Stouffer, R. J. Timescales of climate response. *J. Clim.* **17**, 209–217 (2004).
4. Li, C., von Storch, J.-S. & Marotzke, J. Deep-ocean heat uptake and equilibrium climate response. *Clim. Dynam.* **40**, 1071–1086 (2013).
5. Armour, K. C., Bitz, C. M. & Roe, G. H. Time-varying climate sensitivity from regional feedbacks. *J. Clim.* **26**, 4518–4534 (2013).
6. Collins, M. *et al.* in *Climate Change 2013: The Physical Science Basis* (eds Stocker, T. F. *et al.*) 1029–1136 (IPCC, Cambridge Univ. Press, 2013).
7. Marshall, J. *et al.* The ocean’s role in polar climate change: asymmetric Arctic and Antarctic responses to greenhouse gas and ozone forcing. *Phil. Trans. R. Soc. A* **372**, 20130040 (2014).
8. Masson-Delmotte, V. *et al.* in *Climate Change 2013: The Physical Science Basis* (eds Stocker, T. F. *et al.*) 383–464 (IPCC, Cambridge Univ. Press, 2013).
9. Xie, S.-P. *et al.* Global warming pattern formation: sea surface temperature and rainfall. *J. Clim.* **23**, 966–986 (2010).
10. Yin, J. *et al.* Different magnitudes of projected subsurface ocean warming around Greenland and Antarctica. *Nature Geosci.* **4**, 524–528 (2011).
11. Gent, P. R. The Gent-McWilliams parameterization: 20/20 hindsight. *Ocean Modelling* **39**, 2–9 (2011).

12. Salée, J.-B. *et al.* Assessment of Southern Ocean mixed-layer depths in CMIP5 models: historical bias and forcing response. *J. Geophys. Res.* **118**, 1845–1862 (2013).
13. Kirkman, C. H. & Bitz, C. M. The effect of the sea ice freshwater flux on Southern Ocean temperatures in CCSM3: deep-ocean warming and delayed surface warming. *J. Clim.* **24**, 2224–2237 (2011).
14. Xie, P. & Vallis, G. K. The passive and active nature of ocean heat uptake in idealized climate change experiments. *Clim. Dynam.* **38**, 667–684 (2012).
15. Bintanja, R., van Oldenborgh, G. J., Drijfhout, S. S., Wouters, B. & Katsman, C. A. Important role for ocean warming and increased ice-shelf melt in Antarctic sea-ice expansion. *Nature Geosci.* **6**, 376–379 (2013).
16. Thompson, D. W. *et al.* Signatures of the Antarctic ozone hole in Southern Hemisphere surface climate change. *Nature Geosci.* **4**, 741–749 (2011).
17. Oke, P. R. & England, M. H. Oceanic response to changes in the latitude of the Southern Hemisphere subpolar westerly winds. *J. Clim.* **17**, 1040–1054 (2004).
18. Fyfe, J. C., Saenko, O. A., Zickfeld, K., Eby, M. & Weaver, A. J. The role of poleward-intensifying winds on Southern Ocean warming. *J. Clim.* **20**, 5391–5400 (2007).
19. Hutchinson, D. K., England, M. H., Santoso, A. & Hogg, A. M. Interhemispheric asymmetry in transient global warming: the role of Drake Passage. *Geophys. Res. Lett.* **40**, 1587–1593 (2013).
20. Korhonen, H. *et al.* Aerosol climate feedback due to decadal increases in Southern Hemisphere wind speeds. *Geophys. Res. Lett.* **37**, L02805 (2010).
21. Marshall, J. & Speer, K. Closure of the meridional overturning circulation through Southern Ocean upwelling. *Nature Geosci.* **5**, 171–180 (2012).
22. Karsten, R. H. & Marshall, J. Constructing the residual circulation of the ACC from observations. *J. Phys. Oceanogr.* **32**, 3315–3327 (2002).
23. Reynolds, R. W., Rayner, N. A., Smith, T. M., Stokes, D. C. & Wang, W. An improved *in situ* and satellite SST analysis for climate. *J. Clim.* **15**, 1609–1625 (2002).
24. Yu, L. & Weller, R. A. Objectively analyzed air-sea heat fluxes for the global ice-free oceans (1981–2005). *Bull. Am. Meteorol. Soc.* **88**, 527–539 (2007).
25. Good, S. A., Martin, M. J. & Rayner, N. A. EN4: quality controlled ocean temperature and salinity profiles and monthly objective analyses with uncertainty estimates. *J. Geophys. Res.* **118**, 6704–6716 (2013).
26. Ishii, M. & Kimoto, M. Reevaluation of historical ocean heat content variations with time-varying XBT and MBT depth bias corrections. *J. Oceanogr.* **65**, 287–299 (2009).
27. Gille, S. T. Decadal-scale temperature trends in the Southern Hemisphere ocean. *J. Clim.* **21**, 4749–4765 (2008).
28. Rhein, M. *et al.* in *Climate Change 2013: The Physical Science Basis* (eds Stocker, T. F. *et al.*) 255–316 (IPCC, Cambridge Univ. Press, 2013).
29. Church, J. A. *et al.* in *Understanding Sea Level Rise and Variability* (eds Church, J. A. *et al.*) 143–176 (Blackwell, 2010).
30. Sutton, P. & Roemmich, D. Decadal steric and sea surface height changes in the Southern Hemisphere. *Geophys. Res. Lett.* **38**, L08604 (2011).
31. Durack, P. J., Gleckler, P. J., Landerer, F. W. & Taylor, K. E. Quantifying underestimates of long-term upper-ocean warming. *Nature Clim. Change* **4**, 999–1005 (2014).
32. Taylor, K. E., Stouffer, R. J. & Meehl, G. A. An overview of CMIP5 and the experimental design. *Bull. Am. Meteorol. Soc.* **93**, 485–498 (2012).
33. Cai, W., Cowan, T., Godfrey, S. & Wijffels, S. Simulations of processes associated with the fast warming rate of the southern midlatitude ocean. *J. Clim.* **23**, 197–206 (2010).
34. Kuhlbrodt, T. & Gregory, J. M. Ocean heat uptake and its consequences for the magnitude of sea level rise and climate change. *Geophys. Res. Lett.* **39**, L18608 (2012).
35. Frölicher, T. L. *et al.* Dominance of the Southern Ocean in anthropogenic carbon and heat uptake in CMIP5 models. *J. Clim.* **28**, 862–886 (2015).
36. Ferrari, R. & Ferreira, D. What processes drive the ocean heat transport? *Ocean Modelling* **38**, 171–186 (2011).
37. Screen, J. A., Gillett, N. P., Stevens, D. P., Marshall, G. J. & Roscoe, H. K. The role of eddies in the Southern Ocean temperature response to the southern annular mode. *J. Clim.* **22**, 806–818 (2009).
38. Bitz, C. M. & Polvani, L. M. Antarctic climate response to stratospheric ozone depletion in a fine resolution ocean climate model. *Geophys. Res. Lett.* **39**, L20705 (2012).
39. Ferreira, D., Marshall, J., Bitz, C. M., Solomon, S. & Plumb, A. Antarctic Ocean and sea ice response to ozone depletion: a two timescale problem. *J. Clim.* **28**, 1206–1226 (2015).
40. Sigmond, M. & Fyfe, J. C. The Antarctic sea ice response to the ozone hole in climate models. *J. Clim.* **27**, 1336–1342 (2014).
41. Marshall, J., Hill, C., Perelman, L. & Adcroft, A. Hydrostatic, quasi-hydrostatic, and nonhydrostatic ocean modeling. *J. Geophys. Res.* **102**, 5733–5752 (1997).
42. Marshall, J., Adcroft, A., Hill, C., Perelman, L. & Heisey, C. A finite-volume, incompressible Navier Stokes model for studies of the ocean on parallel computers. *J. Geophys. Res.* **102**, 5753–5766 (1997).
43. Marshall, J. *et al.* The ocean's role in the transient response of climate to abrupt greenhouse gas forcing. *Clim. Dynam.* **44**, 2287–2299 (2015).
44. Donohoe, A., Armour, K. C., Pendergrass, A. G. & Battisti, D. S. Shortwave and longwave radiative contributions to global warming under increasing CO<sub>2</sub>. *Proc. Natl Acad. Sci. USA* **111**, 16700–16705 (2014).
45. Banks, H. T. & Gregory, J. M. Mechanisms of ocean heat uptake in a coupled climate model and the implications for tracer based predictions of ocean heat uptake. *Geophys. Res. Lett.* **33**, L07608 (2006).
46. Downes, S. M., Bindoff, N. L. & Rintoul, S. R. Impacts of climate change on the subduction of mode and intermediate water masses in the Southern Ocean. *J. Clim.* **22**, 3289–3302 (2009).
47. Gille, S. T. Meridional displacement of the Antarctic Circumpolar Current. *Phil. Trans. R. Soc. A* **372**, 20130273 (2014).
48. Swart, N. C. & Fyfe, J. C. The influence of recent Antarctic ice sheet retreat on simulated sea ice area trends. *Geophys. Res. Lett.* **40**, 4328–4332 (2013).
49. Pauling, A. G., Bitz, C. M., Smith, I. J. & Langhorne, P. J. The response of the Southern Ocean and Antarctic sea ice to fresh water from ice shelves in an Earth System Model. *J. Clim.* **29**, 1655–1672 (2016).

## Acknowledgements

The authors thank R. Abernathy, C. Bitz, S. Emerson, Y. Kostov, L.-P. Nadeau, L. Polvani, P. Rhines, G. Roe, L. Thompson and L. Zanna for enlightening feedback; and J.-M. Campin and G. Forget for technical help. The authors are grateful for support from the National Science Foundation through grants OCE-1259388 (J.R.S.), OCE-1338814 (J.M.), OCE-1523641 (K.C.A.) and PLR-1341497 (E.R.N.); from the National Aeronautics and Space Administration through award NNX11AL79G (K.C.A.); and from the Joint Program on the Science and Policy of Global Change, which is funded by a number of federal agencies and a consortium of 40 industrial and foundation sponsors (J.R.S.).

## Author contributions

K.C.A. performed the analyses and wrote the manuscript. J.R.S. performed the ocean-only simulations and associated diagnostics. All authors contributed to the design of the study and interpretation of the results.

## Additional information

Supplementary information is available in the [online version of the paper](#). Reprints and permissions information is available online at [www.nature.com/reprints](http://www.nature.com/reprints). Correspondence and requests for materials should be addressed to K.C.A.

## Competing financial interests

The authors declare no competing financial interests.

## Methods

**Observations.** SST trends since 1950 are calculated from NOAA's Extended Reconstructed Sea Surface Temperature version 3b (ERSST; ref. 50) as linear trends over 1950–2012. SST trends stated in the text are calculated poleward of 50° S (the approximate area south of the ACC), between 50° S and 40° S (the area just north of the ACC), and over the global ocean. Linear SST trends over 1982–2012 (Fig. 1a) are calculated from NOAA's Optimum Interpolation Sea Surface Temperature version 2 (OISST; ref. 23). Linear SHF trends (Fig. 1b) are calculated from the Objectively Analyzed air–sea Flux for the Global Oceans Project<sup>24</sup> data set (OAFlux; see Supplementary Information for a comparison to other observational data sets). Ocean potential temperature trends and heat storage over 1982–2012 and climatological ocean salinity over 1950–2012 (Fig. 1c,d) are calculated using the Met Office Hadley Centre's EN4 version 1.1 (ref. 25). The EN4 temperature and heat storage trends are consistent with those calculated from the Ishii subsurface temperature data set<sup>26</sup> (Fig. 1c), ocean reanalyses, and satellite altimetry observations of sea-level rise (Supplementary Information).

**CMIP5 simulations.** Figure 2a–e shows CMIP5 'Historical' (1982–2005) simulations and their continuation under RCP8.5 (2006–2012). The simulations are driven with historical changes in well-mixed GHGs, aerosols, and stratospheric ozone depletion. Linear trends over 1982–2012 are calculated for SST, SHF and ocean potential temperature, whereas ocean heat uptake is calculated as the integrated SHF over 1982–2012; anomalous ocean heat storage and OHT are averages over 1982–2012 (see below). Figure 2f–j shows CMIP5 simulations of abrupt quadrupling of atmospheric CO<sub>2</sub> above pre-industrial levels. Anomalous SST, SHF, ocean potential temperature and heat storage are calculated from 31-year means centred at 100 years after CO<sub>2</sub> quadrupling, whereas ocean heat uptake is calculated as the integrated SHF over the 100 years; anomalous OHT is an average over the 100 years (see below). To account for model drift, we remove the linear trend over the corresponding years of each model's pre-industrial control simulations from all variables for both the historical and CO<sub>2</sub> quadrupling simulations. We include all models (12 in total) that provide output for the net sea-surface heat flux (below sea ice), which is necessary to accurately calculate ocean heat uptake and OHT anomalies: ACCESS1-0, bcc-csm1-1, CCSM4, CMCC-CM, CNRM-CM5, CSIRO-Mk3-6-0, EC-EARTH, GFDL-ESM2G, MIROC5, MPI-ESM-LR, MRI-CGCM3, and NorESM1-M.

We calculate the anomalous OHT for the CMIP5 models as a residual between the integrated SHF anomaly and ocean heat storage. Uncertainty ranges stated in the text and shown in Fig. 2c,d,h,i are  $\pm 1$  standard deviation across the models. The standard diagnostic for the overturning streamfunction in the CMIP5 models is calculated on depth coordinates, and is thus biased by tilting gyre circulations. To remove these gyre effects, we calculate the residual-mean MOC on isopycnal surfaces and then remap to depth coordinates within a climate model for which we had the necessary output (the National Center for Atmospheric Research's CCSM4; shown in Fig. 2e,j). For consistency, we show CCSM4's total, residual-mean advection, and diffusive OHT components (black lines on Fig. 2d,i).

**Ocean-only GCM simulations.** The MITgcm model is configured with a hybrid latitude–longitude and cubed sphere configuration, realistic bathymetry, 1° horizontal resolution and 50 vertical levels. The eddy diffusivity is set equal to a constant value of 850 m<sup>2</sup> s<sup>-1</sup>, and diapycnal mixing is set to a constant value of 10<sup>-5</sup> m<sup>2</sup> s<sup>-1</sup>. The model is initialized with climatological ocean temperature and

salinity data<sup>51</sup>, and driven with a repeating annual cycle of atmospheric forcing from the Coordinated Ocean-ice Reference Experiment (CORE) 1 protocol<sup>52</sup> for a 'spin-up' period of 310 years before the climate forcing simulations. Further model diagnostics and simulation details can be found in ref. 43. Over this 'spin-up' integration, net air–sea fluxes are computed using bulk formulae; for stability, surface salinity is restored on a timescale of 250 days. Once steady state is achieved, we store all sea-surface buoyancy and momentum fluxes at daily resolution. We then drive the model again by prescribing these stored, steady-state and annually repeating fluxes (now without bulk formulae or salinity restoring), thus producing the 'control' integration against which all climate change simulations are compared. Climate forcings are applied concurrently with these stored fluxes and with a spatially uniform 'radiative feedback' on SST anomalies (relative to the control), as described in the main text. The SST below sea ice evolves according to these same boundary conditions, and is thus able to go above the freezing point. Because this framework does not capture increased poleward atmospheric heat transport with global warming, surface heat uptake over the SO (Fig. 3b) is limited by the 4 W m<sup>-2</sup> radiative forcing we have applied, and is thus smaller in magnitude than that simulated by the CMIP5 GCMs (Fig. 2g).

Anomalous SST, SHF, ocean potential temperature and heat storage are calculated at 100 years after CO<sub>2</sub> forcing, whereas ocean heat uptake is calculated as the integrated SHF over the 100 years; anomalous OHT is an average over the 100 years. We calculate the residual-mean MOC for the MITgcm model on isopycnal surfaces and then remap to depth coordinates. The MOC shown in Fig. 3e,j is from the MITgcm control simulation; anomalies in the MOC under GHG and westerly wind forcing are shown in Supplementary Figs 10 and 12, respectively.

For the passive-tracer simulation, the tracer has units of temperature but does not affect ocean circulation in any way. The passive tracer is initialized to the control ocean temperature distribution, and is forced and damped uniformly at the sea surface with magnitudes  $F = 4 \text{ W m}^{-2}$  and  $\lambda = 1 \text{ W m}^{-2} \text{ } ^\circ\text{C}^{-1}$ , respectively, just as in the GHG-forcing scenario.

**Code availability.** The MITgcm source code can be accessed at <http://mitgcm.org>.

**Data availability.** NOAA's ERSST data set is available at <http://www.esrl.noaa.gov/psd/data/gridded/data.noaa.ersst.html>. NOAA's OISST data set is available at <http://www.esrl.noaa.gov/psd/data/gridded/data.noaa.oisst.v2.html>. The Hadley Centre's EN4 data set is available at <http://www.metoffice.gov.uk/hadobs/en4>. The OAFlux data set is available at <http://oafux.who.edu>. The CMIP5 data were downloaded through the Program for Climate Model Diagnostics and Intercomparison's Earth System Grid ([http://cmip-pcmdi.llnl.gov/cmip5/data\\_portal.html](http://cmip-pcmdi.llnl.gov/cmip5/data_portal.html)). The data that support the findings of this study are available from the corresponding author on request.

## References

- Smith, T. M., Reynolds, R. W., Peterson, T. C. & Lawrimore, J. Improvements to NOAA's historical merged land–ocean temperature analysis (1880–2006). *J. Clim.* **21**, 2283–2296 (2008).
- Steele, M., Morley, R. & Ermold, W. PHC: a global ocean hydrography with a high quality Arctic Ocean. *J. Clim.* **14**, 2079–2087 (2001).
- Griffies, S. *et al.* Coordinated Ocean-ice Reference Experiments (COREs). *Ocean Modelling* **26**, 1–46 (2009).